Single-step Planar Surface Extraction from Range Images

Shanmugalingam Suganthan, Sonya Coleman
School of Computing and Intelligent Systems
University of Ulster, Londonderry, UK
S.Suganthan@Ulster.ac.uk , SA.Coleman@Ulster.ac.uk

Bryan Scotney
School of Computing & Information Engineering
University of Ulster, Coleraine, UK
BW.Scotney@Ulster.ac.uk

Abstract

The volume of raw range image data that is required to represent just a single scene can be extensive; hence direct interpretation of range images can incur a very high computational cost. Range image segmentation and feature extraction have been identified as mechanisms to produce more compact scene representations and hence enable less costly scene interpretation for applications such as object recognition and robot navigation. We present a new approach to multi-scale edge and planar surface detection in range images that can be used directly with any range data, regardless of whether the data have regular or irregular spatial distribution. The approach is evaluated with respect to accuracy of both edge location and planar surface representation. The contribution of our approach is that only a single application of our operator is necessary to both extract object edges and determine representations of the corresponding planar object surfaces.

1. Introduction

The earliest developments of object recognition systems for range data concentrate primarily on polyhedral objects, progressing later to segmentation of curved objects [17]. Advances were then made with the development of segmentation methods to preserve the location and amplitude of the feature output as well as noise reduction [6,7,14,25]. The use and processing of range data continues to be an active area of research with, for example, advances in 3-D face recognition [5,22], face modelling [11] and object extraction[12,26].

For many years multi-scale approaches to feature extraction have been investigated, as it is well known that the strength of any feature in an image may depend on the scale at which the appropriate detection operator is applied. Whilst much research has been carried out to develop edge detection methods for range image data, little has focused on the area of multiscale, or adaptive, edge detection methods. When edges in an image that occur over a range of scale are extracted at only one scale, localization error or false edges may be introduced. Currently multi-scale approaches to feature extraction in range data include those in [9, 18, 19, 20].

Although range image data provide us with an almost 3-D representation of a scene, each range image requires a large amount of data, and hence we often apply image processing algorithms to decompose the image into a 2-D representation. However, such an approach is not appropriate in situations where a robot is navigating through a 3-D environment [24]. For example, there may in a chair in the robot's path, but without 3-D information, the robot would not know that the seat of the chair was much closer than the chair back. In addition 3-D representations of objects are also useful in a wide range of applications, such as architecture, visualization [24], robotic bin picking [15], and automatic unloading of piled box-like objects [16]. An approach to providing a rich representation of a 3-D scene, whilst reducing storage overhead, is the extraction of object surfaces from 3-D data in addition to edges. Existing methods for planar surface extraction include [2, 21, 23, 24].

Multi-scale considerations combined with the need to handle the potentially irregular spatial distribution of range data make it necessary to consider operator adaptivity with respect to both scale and shape. Directional derivative operators play a key role in many feature detection algorithms, and we present a new multi-scale approach to directional derivative operators that have the ability to adapt their shape in accordance with the local data distribution, both regular and irregular. The purpose is to develop representations of object surfaces and the relationships between them that can be useful in guiding the behaviour of a robot within its environment. The contribution of our approach is that only a single application of our operator is necessary to both extract object edges and determine a representation of the corresponding planar object surfaces.

2. Irregular Direction Derivative Operators

In this section we described the design procedure for our shape adaptive directional derivative operators.

2.1. Data Representation

We consider a range image to be represented by a spatially irregular sample of values of a continuous function $U(x, y)$ of image depth on a domain Ω. Our operator design is based on the use of a quadrilateral mesh as illustrated in Figure 1, in which the nodes are the sample points. We approximately represent the range image function U by a function

$$U(x,y) = \sum_{n=1}^{N} U_n \phi_n(x,y) \tag{1}$$

Where the basis functions $\phi_m(x, y)$ are piecewise bilinear on each quadrilateral element and have support restricted to a neighbourhood centred on node *m* consisting of those four elements that have node *m* as a vertex. Therefore, approximate image representation takes the form of a bilinear polynomial on each element and has the sampled range value U_n at node *n.*

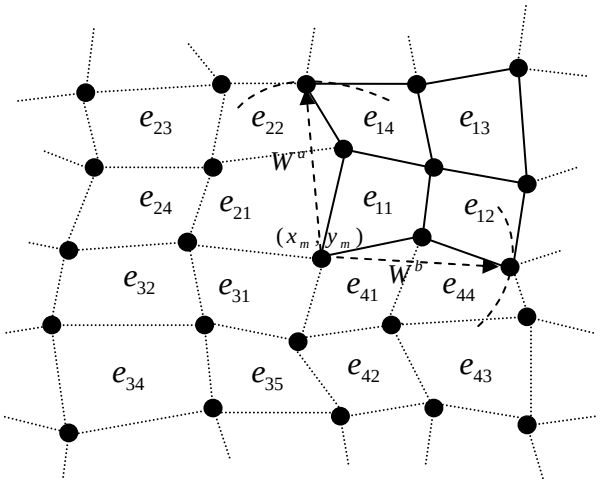

Figure 1. Local 5×5 operator neighbourhood

2.2. Shape Adaptive Operator Design

We describe the framework for construction of the multi-scale directional derivative operators; we use the 5×5 operator, illustrated in Figure 1, as an example. The operators correspond to weak forms in the finite element method [3]: for the directional derivative

$$\partial u / \partial b \equiv \underline{b} \cdot \underline{\nabla} u \tag{2}$$

we may use a test function $v \in H^1(\Omega)$ to define the weak form

$$E(u) = \int_{\Omega} \underline{b} \cdot \underline{\nabla} u v \, d\Omega \tag{3}$$

where $\underline{b} = (\cos\theta, \sin\theta)$ is the unit direction vector.

In our operator design we use a Gaussian test function

$$\psi_m^{\sigma}(x,y) = \frac{1}{2\pi\sigma^2} e^{-\left(\frac{(x-x_m)^2+(y-y_m)^2}{2\sigma^2}\right)} \tag{4}$$

to embrace explicitly size and shape variability. The parameter σ is determined by the local data distribution. The first order functional is then defined as:

$$E_m^{\sigma}(U) = \int_{\Omega_m^{\sigma}} \underline{b}_m \cdot \underline{\nabla} U \psi_m^{\sigma} \, d\Omega_m \tag{5}$$

Within each neighbourhood a different σ parameter is computed for each quadrant of the neighbourhood, enabling the Gaussian test function to adapt to the local area more accurately. The parameter W_{σ}^{m} is chosen as the maximum of W^a and W^b, Euclidean distances, as illustrated in Figure 1, and in each case the quadrant scale parameter $\sigma_m = W_{\sigma}^{m} / 1.96$ ensures that the cross-section of the quadrant through (x_m, y_m) encompasses 95% of the cross-section of the Gaussian.

On a neighbourhood Ω_m^{σ} we consider a locally constant unit vector $\underline{b}_m = (b_{m1}, b_{m2})^T$. Substituting the image representation Equation (1) into the weak form Equation (5) gives

$$E_m^{\sigma}(U) = b_{m1} \sum_{n=1}^{N} K_{mn}^{\sigma} U_n + b_{m2} \sum_{n=1}^{N} L_{mn}^{\sigma} U_n \tag{6}$$

where K_{mn}^{σ} and L_{mn}^{σ} are respectively

$$K_{mn}^{\sigma} = \int_{\Omega_m^{\sigma}} \frac{\partial \phi_n}{\partial x} \psi_m^{\sigma} dx dy \qquad m,n = 1 \ldots N \tag{7}$$

and

$$L_{mn}^{\sigma} = \int_{\Omega_m^{\sigma}} \frac{\partial \phi_n}{\partial y} \psi_m^{\sigma} dx dy \qquad m,n = 1 \ldots N \tag{8}$$

These integrals need be computed only over the neighbourhood Ω_m^{σ}, rather than the entire image domain Ω, since ψ_m^{σ} has support restricted to Ω_m^{σ}. The element integrals K_{mn}^{σ} and L_{mn}^{σ} are actually computed by using an isoparametric mapping to a standard reference element in order to facilitate the integration using a simple four-point quadrature rule.

Construction of the operators on an irregular quadrilateral grid differs from that of image processing operators on a typically regular grid in that it is no longer appropriate to build explicitly an entire operator, as each operator throughout an irregular mesh may be different with respect to the operator neighbourhood shape. When using an irregular grid, we work on an element-by-element basis, taking advantage of the flexibility offered by the finite element method as a means of adaptively changing the irregular operator shape to encompass the

data available in any local neighbourhood.

3. Edge Detection on Range Images

The problem of edge detection when using range images is different from that when using intensity images in that standard thresholding approaches are no longer appropriate.

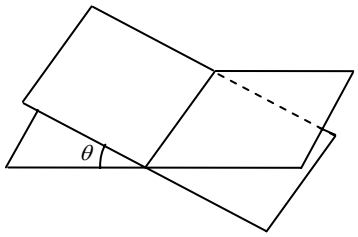

Figure 2. Dihedral Angle

We propose a technique based on the dihedral angle between two surfaces. This angle can be seen by looking at the planes "edge on", i.e., along their line of intersection and is represented by θ in Figure 2. The dihedral angle between the two planes that have unit normal vectors $\vec{N}_{11}$ and $\vec{N}_{22}$ is computed as the scalar product of the normals. Let $z = U(x, y)$, the normal vector $\vec{N}$ can be defined as $\vec{N} = \frac{\partial U}{\partial x}\underline{i} + \frac{\partial U}{\partial y}\underline{j} - \underline{k}$. For simplicity we define the derivatives at point (x_i, y_j) as $x'_{ij} = \left(\frac{\partial U}{\partial x}\right)_{i,j}$, $y'_{ij} = \left(\frac{\partial U}{\partial y}\right)_{i,j}$ Therefore the unit normal vectors $\vec{N}_{11}$ and $\vec{N}_{22}$ of two given points (x_1, y_1) and (x_2, y_2) as illustrated in Figure 3 can be defined as:

$$\vec{N}_{11} = \frac{x'_{11}}{\sqrt{x'^2_{11} + y'^2_{11} + 1}}\underline{i} + \frac{y'_{11}}{\sqrt{x'^2_{11} + y'^2_{11} + 1}}\underline{j} - \frac{1}{\sqrt{x'^2_{11} + y'^2_{11} + 1}}\underline{k} \quad (9)$$

$$\vec{N}_{22} = \frac{x'_{22}}{\sqrt{x'^2_{22} + y'^2_{22} + 1}}\underline{i} + \frac{y'_{22}}{\sqrt{x'^2_{22} + y'^2_{22} + 1}}\underline{j} - \frac{1}{\sqrt{x'^2_{22} + y'^2_{22} + 1}}\underline{k} \quad (10)$$

Then

$$\vec{N}_{11} \cdot \vec{N}_{22} = \left|\vec{N}_{11}\right|\left|\vec{N}_{22}\right| \cos\theta = \cos\theta \quad (11)$$

If the dihedral angle θ is zero then the two points are on the same plane and hence no features are detected. However if the dihedral angle θ is non-zero, then the two points are on different planes and a feature is therefore found. We search for features in both the *x* and *y* directions. Therefore, we calculated the dihedral angle θ_{x_i} between the points (x_{i-1}, y_j) and (x_{i+1}, y_j), and if $\theta_{x_i} \neq 0$ we denoted a feature at point (x_i, y_j). Similarly, we calculate θ_{y_j} between the points (x_i, y_{j-1}) and (x_i, y_{j+1}), and if $\theta_{y_j} \neq 0$ we denoted a feature at point (x_i, y_j). It should be noted that in theory when $\theta_{ij} \neq 0$ an edge is found; however, due to the present of noise, this is not always the case, and hence we introduce thresholding. The algorithm can be generalised as follows: At point (x_i, y_j) compute

$$\vec{N}_{i-1,j} \cdot \vec{N}_{i+1,j} = \cos\theta_{x_i} \quad (12)$$

$$\vec{N}_{i,j-1} \cdot \vec{N}_{i,j+1} = \cos\theta_{y_j} \quad (13)$$

$$\cos\theta_{ij} = \min\left(\cos\theta_{x_i}, \cos\theta_{y_j}\right) \text{ //hence maximising } \theta_{ij} \text{ //} \quad (14)$$

An edge point as E_{ij} is defined if

$$E_{ij} \leftarrow (\cos\theta_{ij} < T) \text{ where } -1 < T \leq 1 \quad (15)$$

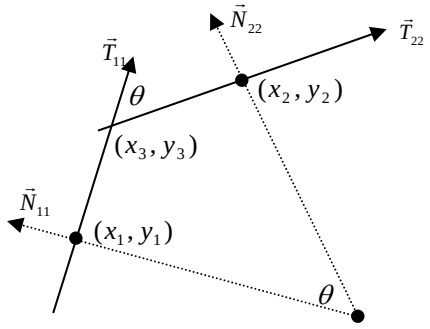

Figure 3. Relations between surface points

3.1. Edge Evaluation

In order to demonstrate the flexibility of the proposed techniques over a range of irregularly distributed range images, we generated a set of synthetic test images for each edge type encountered in a range image: convex roof, concave roof, convex crease, concave crease, jump. Each set corresponds to one of the edge types and is comprised of five images generated using a fixed value for a random spatial location parameter *r*. To generate the images with irregularly distributed data, we create a regularly distributed image and add varying degrees of random values to the *x* and *y* co-ordinates such that $x = x + r_x$, $y = y + r_y$ where $0 \leq r_x \leq N$ and $0 \leq r_y \leq N$ and *N* defines the degree of irregularity.

For evaluation purposes, we use the Figure of Merit measure [1]; we compare the dihedral angle approach to edge finding using the directional derivative 3×3 and 5×5 operators as described in Section 2.2, denoted as 3DA and 5DA respectively, the significant gradient change thresholding approach to edge finding [4], denoted as 3SGC and 5SGC, and the well-known scan-line approximation algorithm [14].

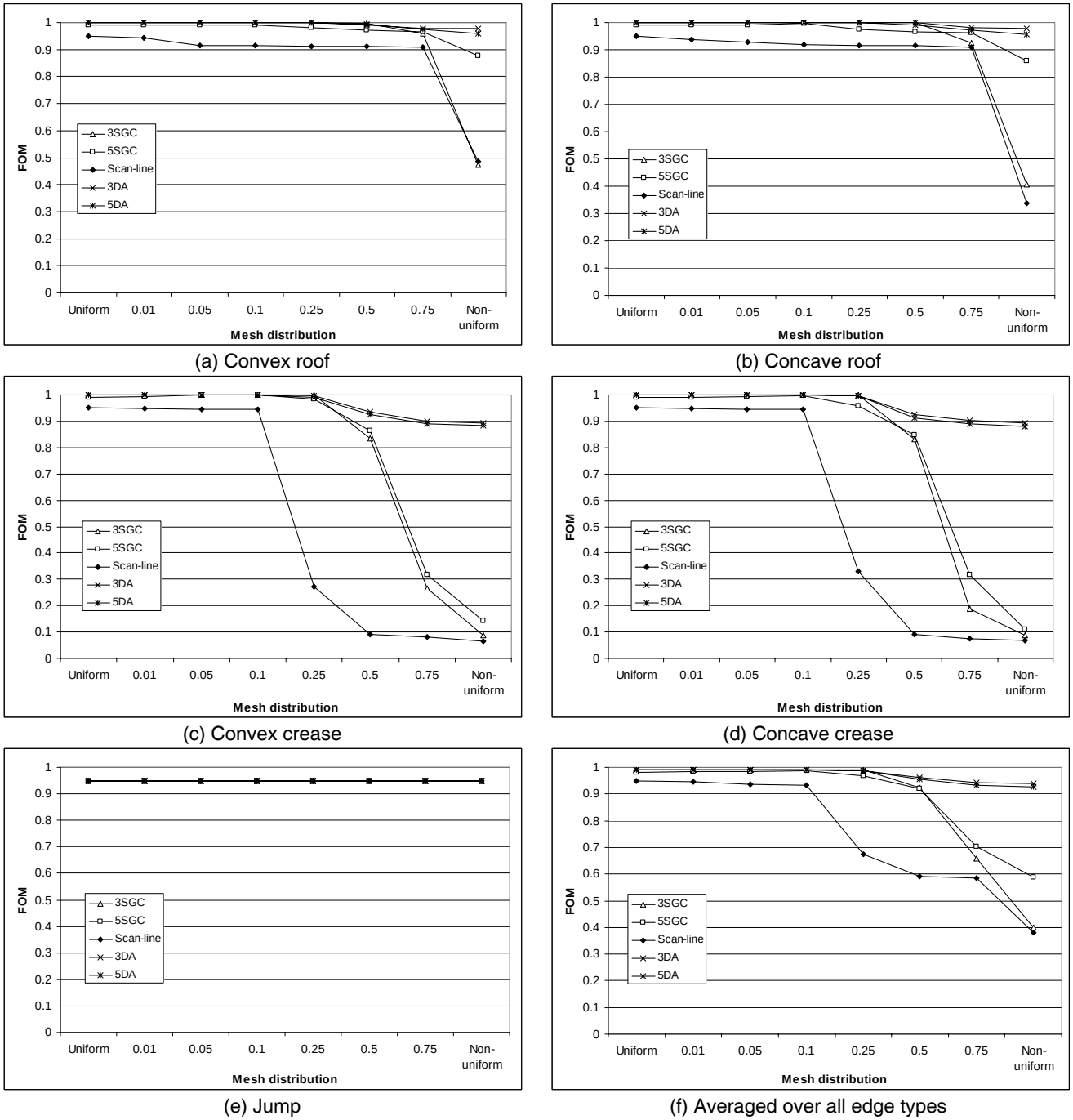

Figure 4. Figure of Merit results for different edge types over a range of data irregularity

In Figure 4 we show results using Figure of Merit (FoM) evaluation technique for an edge within a range image using varying degrees of irregularity and no noise. In each case the threshold value used provides the best FoM; similarly, FoM is computed over all possible parameter combinations for the scan line approach, and again the best value selected. In addition, the results are computed on five randomly generated meshes, comprising five of each range edge type: convex roof, concave roof, convex crease, concave crease, jump, and the best FoM value is averaged for each. In general, these results indicate that our approach works better over range of data irregularity than the well-known scan-line approach. The results also illustrate that the dihedral angle approach to edge finding is more accurate than the significant change approach in [4]. An obvious comparison that should be

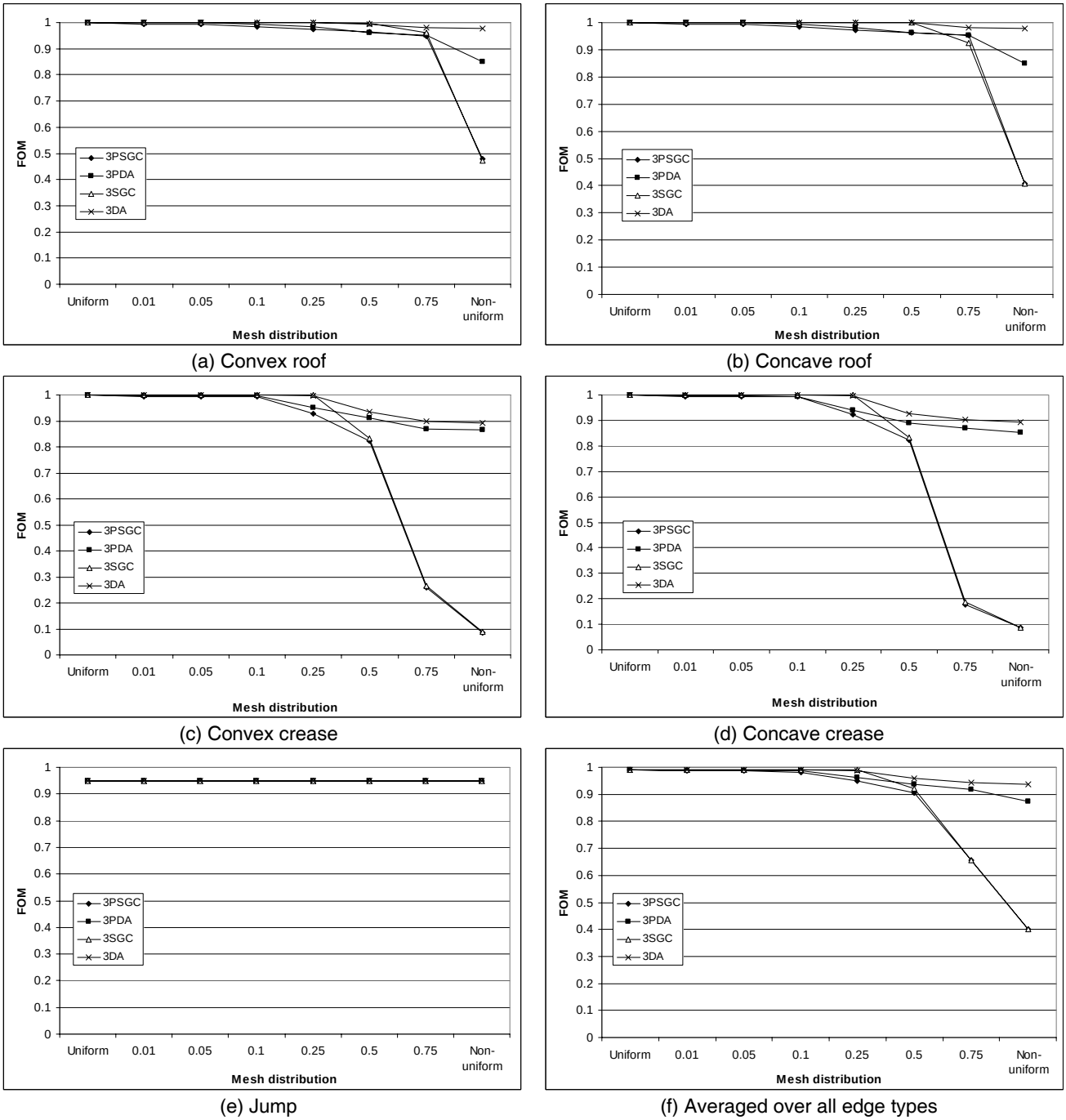

Figure 5. Figure of Merit results for different edge types over a range of data irregularity using original irregular and interpolated range data

made is with the use of regular directional derivative operators applied to regularly distributed data obtained by interpolation. Therefore, for completeness, in Figure 5 we illustrate the results of applying the shape-adaptive 3×3 operator to the original irregular range data (3SGC and 3DA) and the regular 3×3 operator to interpolated (pre-processed) range data (3PSGC and 3PDA). Although we have previously illustrated that the dihedral angle approach (e.g., 3DA) performs better than the significant gradient change approach presented in [4] (e.g., 3SGC), we have illustrated both cases in the interpolated data to show that this still holds true. These processing times would be required for image interpolation that is not required with our proposed algorithm.

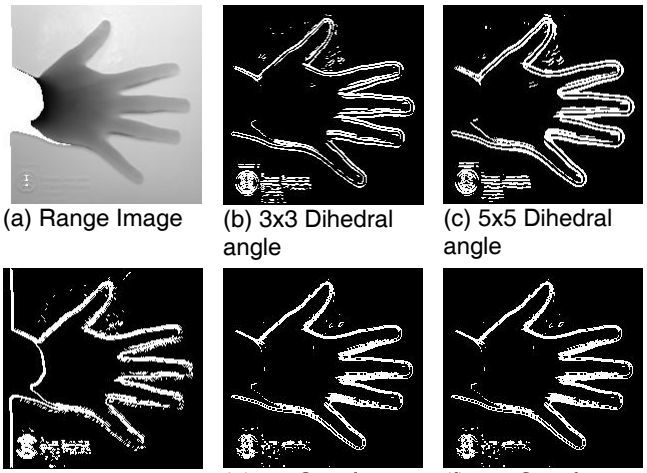

(a) Range Image (b) 3x3 Dihedral angle (c) 5x5 Dihedral angle

(d) Scan line approach [14] (e) 3x3Significant Gradient change (f) 5x5 Significant Gradient change

Figure 6. Comparative Edge map

Although the Figure of Merit graphs provide an indication of the accuracy of the dihedral angle approach, results show clearly that error is introduced by image interpolation. It should also be noted that additional the results are not always very discriminating. Therefore, in addition to presenting quantitative evaluation, we illustrate our technique using a real range image. The feature maps illustrated in Figure 6 support the quantitative evaluation by demonstrating that the proposed dihedral angle provides better feature maps than the other techniques shown; this is most evident in Figure 6(b-c), where the depth of the fingers is made more apparent.

4. Polygon Extraction

Representation of an environment via raw range image data may require an extensive amount of data to be stored for each individual image. This large volume of data makes direct interpretation computationally costly. Range image feature extraction and segmentation have been identified as a less costly means of scene representation and can be used in applications such as object recognition. However, reducing a 3-D image to a 2-D image is not always appropriate, particularly where 3-D tasks are to be performed based on the reduced data representation. Therefore, in this section we outline how output from the proposed directional derivative operators can be used to both extract and characterise planar surfaces using a process of polygon extraction. A 3D range data set is thus reduced to a set of finite line segments (object boundaries) and a corresponding set of bounded planar surfaces (object surfaces).

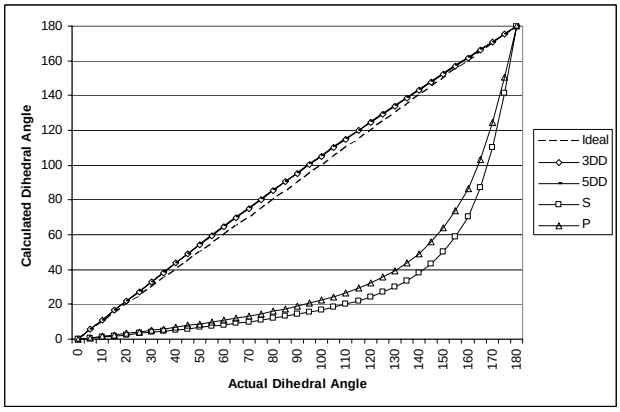

Figure 7. Dihedral angle response

As described in Section 3, the directional derivative operators are used to detect the boundaries of the planar surfaces by computing and thresholding the dihedral angle. Then a labelling algorithm [10] within Matlab is used to identify each polygon, as illustrated in Figure 8. This algorithm is based on random selection of seed points and region growing until sets of boundary points that form closed (object) boundaries are identified.

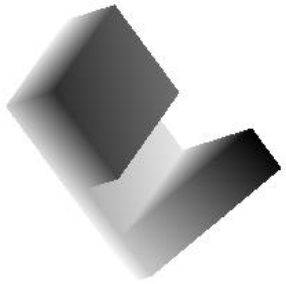

(a) Range Image

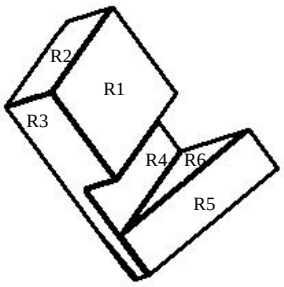

(b) Corresponding region labelling (region boundaries found using Dihedral angle approach with 3x3 directional derivative)

Figure 8. Polygon Extraction

For each labelled polygon, the surface normal direction has already been computed at each range image data point

during the process of edge detection. From these normal directions within each segmented region we then formulate a representation of the corresponding (object) surface in terms of a plane characterised by the "average" surface normal vector:

$$\vec{N}_{R_i} = \frac{1}{n_{R_i}} \sum_{r,c \in R_i} \left(\frac{\partial U}{\partial x} \right)_{r,c} \underline{i} + \frac{1}{n_{R_i}} \sum_{r,c \in R_i} \left(\frac{\partial U}{\partial y} \right)_{r,c} \underline{j} - \underline{k} \qquad (16)$$

Here n_{R_i} is number of range image data points within region R_i.

Polygon	Plane equation using 3x3	Plane equation using 5x5
R_1	$\vec{N}_{R_1} = 0.33\underline{i} + 0.08\underline{j} + \underline{k}$	$\vec{N}_{R_1} = 0.33\underline{i} + 0.07\underline{j} + \underline{k}$
R_2	$\vec{N}_{R_2} = -2.86\underline{i} + 2.99\underline{j} + \underline{k}$	$\vec{N}_{R_2} = -2.88\underline{i} + 2.85\underline{j} + \underline{k}$
R_3	$\vec{N}_{R_3} = -1.68\underline{i} - 1.83\underline{j} - \underline{k}$	$\vec{N}_{R_3} = -1.62\underline{i} - 1.75\underline{j} - \underline{k}$
R_4	$\vec{N}_{R_4} = 0.33\underline{i} + 0.08\underline{j} - \underline{k}$	$\vec{N}_{R4} = 0.34\underline{i} + 0.06\underline{j} - \underline{k}$
R_5	$\vec{N}_{R_5} = -0.49\underline{i} - 0.70\underline{j} - \underline{k}$	$\vec{N}_{R_5} = -0.47\underline{i} - 0.66\underline{j} - \underline{k}$
R_6	$\vec{N}_{R_6} = -2.86\underline{i} + 2.99\underline{j} - \underline{k}$	$\vec{N}_{R_6} = -2.90\underline{i} + 2.86\underline{j} - \underline{k}$

Table 1. The sample image plane equations

In order to demonstrate the flexibility of the proposed technique, we generated a set of roof edges with dihedral angle θ where $0^\circ \le \theta \le 180^\circ$ at intervals of 5°. Figure 7 shows the dihedral angle response at each planar surface separation angle. For comparison we show the responses for the 3×3 and 5×5 directional derivative (3DD and 5DD respectively), Prewitt (P) and Sobel (S), with the dashed line representing the ideal response. The direction derivative operators appear to provide accurate dihedral angle values over the full range of planar surface separations.

Planes	Dihedral angle using 3x3 operators	Dihedral angle using 5x5 operators
R_1 - R_2	93.83	93.44
R_1 - R_3	96.15	97.23
R_1 - R_4	180.00	179.29
R_2 - R_3	91.75	93.77
R_3 - R_4	96.15	97.29
R_3 - R_5	151.72	151.28
R_4 - R_6	93.83	92.65
R_5 - R_6	93.27	94.92

Table 2. Dihedral angles between the Polygons in Figure 8(b)

As an illustration of application to range image data, Table 1 provides plane equations for each of the planar surfaces labelled in Figure 8(b), using both the 3×3 and 5×5 shape-adaptive directional derivative operators; each operator provides a plane equation for each segment, and hence we can represent a range images as a reduced data set containing only edge points and planar surface equations.

Table 2 provides dihedral angles computed between the polygons identified in Figure 8(b), which are computed directly from the surface unit normal vectors in Table 1. Such planar surface separation information is useful for applications such as robot picking, where a robot arm needs to know how much grasp is necessary, or when determining whether structures are parallel [24].

5. Conclusion

The purpose of extracting planar surfaces from range image data is to generate a compact scene representation that retains 3D scene information that is important for tasks, such as localisation and navigation that are essentially 3D in nature. The extraction of planar surfaces is often achieved through a two-step approach: one algorithm is used for the extraction of (object) edges; another algorithm is used for the extraction of the planar (object) surfaces. This is evident in approaches such as [23], where a Sobel operator is applied to find edges prior to plane extraction, and [8], where step and roof edges are detected as a pre-processing step before surface extraction is achieved. In [23], an additional pre-processing step is used to generate data on a regular rectangular grid via bilinear interpolation. We have presented a family of multi-scale directional derivative operators that can be applied directly to range data, regardless of whether the spatial distribution is regular or irregular. Through the single-step application of such operators, we acquire all of the necessary output to enable both edge finding and planar surface extraction, without the application of additional techniques or the need for pre-processing. An overview of our algorithm is:

1. Apply the (adaptively sized) directional derivative operator to compute $\frac{\partial U}{dx}$ and $\frac{\partial U}{dy}$ directly over the set of raw range data.
2. Compute the dihedral angle to determine edge points using $\frac{\partial U}{dx}$ and $\frac{\partial U}{dy}$
3. Determine closed polygonal regions using the connected components labelling algorithm in [10]
4. Determine plane equation using $\frac{\partial U}{dx}$ and $\frac{\partial U}{dy}$ within each region to characterise each planar surface.

In terms of edge accuracy, we have demonstrated that our approach outperforms the well-known scan-line approach over a range of levels of irregularity. Where the data have irregular spatial distribution, we have also demonstrated the benefits of applying the operators directly to the original data rather than pre-processing the data onto a regular grid. The results shown for (object) planar surface representation demonstrate consistency in the characterisation in terms of the plane equation derived for each region using differently sized adaptive operators. In further work this single-step approach will be tested in an industrial application, such as distinguishing between piled box-like objects [16].

Acknowledgment

This work was supported by the U.K Research Council EPSRC. We would like to thank Professor Horst Bunke for providing us with the code for the scan line approximation algorithm in [14].

References

[1] Abdou, B, Pratt, W.K., "Quantitative Design and Evaluation of Enhancement/ Threshold Edge Detectors", *Proc of the IEEE*, Vol.67, No.5, May 1979

[2] Ashbrook, A.P., Fisher, R.B., Robertson, C., Wergi, N., "Segmentation of Range Data into Rigid Subsets using Planar Surface Patches" *Proc of IEEE ICCV*, pp201-206, 1997.

[3] Becker, E.B., Carey, G.F., and Oden, J.T., *Finite Elements: An Introduction*, Prentice Hall, London, 1981.

[4] Coleman, S.A., Scotney, B.W., Suganthan, S. "Feature Extraction on Range Images – A New Approach", *Proc of IEEE ICRA*, pp.1098-1103, 2007

[5] Colombo, A., Cusano, C., Schettini, R., "Face a 2D+3D Robust Face Recognition System" *Proc of IEEE ICIAP*, pp393-398, 2007

[6] Flynn, P.J., and Jain, A.K., "BONSAI: 3D Object Recognition Using Constrained Search" *IEEE Trans. Pattern Analysis and Machine Intelligence*, Vol 13, No. 10, pp.1066-1075, 1991.

[7] Goldgof, D.B., et al., "A Curvature-Based Approach to Terrain Recognition" *IEEE Trans. Pattern Analysis and Machine Intelligence*, Vol 11, pp.1213-1217, 1989.

[8] Gotardo, P.F.U, Bellon, O.R.P., Silva, L., "Range Image Segmentation by Surface Extraction Using an Improved Robust Estimator" *Proc of IEEE CVPR*, pp33-38, Vol. 2, 2003.

[9] Gunsel, B., et al., "Reconstruction and boundary detection of range and intensity images using multiscale MRF representations" *Computer Vision and Image Understanding*, Vol. 63, pp353-366, 1996.

[10] Haralick, R.M., Shapiro, L.G., *Computer and Robot Vision*, Volume I, Addison-Wesley, 1992, pp. 28-48

[11] Huq, S., Abidi, B., Abidi, M., "Stereo-based 3D Face Modelling using Annealing in Local Energy Minimization" *Proc of IEEE ICIAP*, pp265-270, 2007.

[12] Jain, A.K., Dorai, C., "3D Object Recognition: Representation and Matching" *Statistics and Computing, Kluwer*, Vol. 10, pp167-182, 2000.

[13] Jiang, X. Y., and Bunke, H., "Fast Segmentation of Range Images into Planar Regions by Scan Line Grouping", *Machine Vision and Applications*, Vol. 7, No. 2, pp115-122, 1994.

[14] Jiang, X., and Bunke, H., "Edge Detection in Range Images Based on Scan Line Approximation" *Computer Vision and Image Understanding*, Vol.73, No.2 1999, pp. 183-199

[15] Katsoulos, D., Kosmopoulos, D.I., "Superquadric Segmentation in Range Images via Fusion of Region and Boundary Information", *IEEE Trans Pattern Analysis and Machine Intelligence*, Accepted for publication in 2007.

[16] Katsoulos, D., Werber, A., "Edge Detection in Range Images of Piled Box-Like Objects" *Proc of ICPR*, pp80-84, Vol. 2, 2004.

[17] Kaveti, S., et al., "Second-Order Implicit Polynomials for segmentation of Range Images." *Pattern Recognition*, Vol. 29, No. 6, pp. 937-949, 1996.

[18] Kazanov, M., "One Approach to Multi-Scale edge Detection" *Proc of IASTED Int Conf Visualization, Imaging and Image Processing*, pp356-360, 2003.

[19] Mazouzi, S., Guessoum, Z., Michel, F., Batouche, M., "A Multi-agent Approach for Range Image Segmentation" *Proc of 5th Int Central and Eastern European Conference on Multi-Agent Systems*, Springer-Verlag, LNAI 4696, pp1-10, 2007.

[20] Parvin, B., and Medioni, G., "Adaptive Multiscale Feature Extraction From Range Data" *Computer Vision Graphics, Image Understanding*, Vol. 45, pp. 346-356, 1989

[21] Pulli, K., Pietikainen, M., "Range Image Segmentation Based on Decomposition of Surface Normals" *Proc of Scandinavian Conference on Image Analysis (SCIA)*, Norway, 1993.

[22] Queirolo, C., Segundo, M.P., Bellon, O., Silva, L., "Noise versus Facial Expression on 3D Face Recognition" *Proc of IEEE ICIAP*, pp171-176, 2007.

[23] Thakoor, N., Jung, S., Gao, J., "Real-time Planar surface Segmentation in Disparity Space" *Proc of IEEE CVPR*, pp1-8, 2007.

[24] Triebel, R., Burgard, W., Dellaert, F., "Using Hierarchical EM to Extract Planes from 3D Range Scans" *Proc of IEEE ICRA*, pp4437-4442, 2005.

[25] Trucco, E., and Fisher, R.B., "Experiments in Curvature-Based Segmentation of Range Data", *IEEE Trans. Pattern Analysis and Machine Intelligence*, Vol 17, No. 2, pp. 177-182, 1995.

[26] Yu, Y., Ferencz, A., Malik, J., "Extracting Objects from Range and Radiance Images" *IEEE Trans on Visualization and Computer Graphics*, Vol. 7, No. 4, pp351-364, 2001.